Tellus (1988), *40B*, 189–204

Microphysical, thermodynamical and dynamical properties as observed in the upper part of a small growing warm cumulus cloud

By PETER MEISCHNER and WERNER BÖGEL, *Institut für Physik der Atmosphäre, Deutsche Forschungs- und Versuchsanstalt für Luft- und Raumfahrt e.V., Oberpfaffenhofen, D-8031 Wessling, FRG*

(Manuscript received 10 July 1987; in final form 28 September 1987)

ABSTRACT

A detailed aircraft case study of the upper part of a growing, warm, nonprecipitating cumulus cloud is presented. Measurements were made for 36 min near actual cloud top. The small and shallow cloud observed over the lower Alps in the summer of 1982 was intensively mixing with environmental air during its growth. A contour presentation of measured cloud droplet spectra shows their variability as related to the dynamical and thermodynamical properties. Two distinctly different structures were observed, i.e., parts being rather homogeneous with respect to microphysics, and microphysically inhomogeneous parts. Microphysical homogeneity was observed in regions characterized by strong upward motion, water vapour saturation and positive buoyancy. Microphysical inhomogeneity was connected with undersaturation and negative buoyancies within upward moving parcels. An air mass budget estimation shows that by the end of the observation time, about 85% of the cloud air near the top consisted of air entrained from the environment during growth. A time constant for turbulent mixing, estimated from observed maximal LWC values and vertical velocities, is of the order of magnitude of reported values.

1. Introduction

The relation between environmental conditions, cloud dynamics and microphysics is still not fully understood. For the liquid water content, discrepancies are reported between observations and model experiments. Observational values are often found to be considerably below the values computed for adiabatic lifting. Furthermore, in natural clouds the precipitation formation process is faster than modelled, when only condensation and the stochastic coalescence mechanisms are taken into account (Warner, 1969; Jonas and Mason, 1982). The explanation for this is that during cloud growth dry environmental air is mixed in which decreases the liquid water content. In addition, the turbulent mixing process tends to broaden the cloud droplet spectra in the early state of cloud formation thus increasing the probability for coalescence.

The current approaches taken for the understanding and simulation of such small scale entrainment and mixing processes in cumulus clouds may be divided into two main categories. One category takes into account a realistic and physically consistent fluid dynamics formulation but does not include the detailed microphysical response (Baker et al., 1984). The other category examines the response of cloud droplet populations when a cloud parcel mixes with dry air under a variety of artificial conditions without focusing on the fluid dynamical consistency (Telford and Chai, 1980; Telford and Wagner, 1980; Telford and Wagner, 1981; Baker and Latham, 1982). In accordance with observations by Paluch (1979) and La Montagne and Telford (1983), the mixed-in air is assumed to originate predominantly from above the cloud top resulting in penetrative downdrafts.

In the model of "inhomogeneous mixing" (Baker and Latham, 1979; Baker et al., 1980;

Blyth et al., 1980; Baker et al., 1982) for example, the entrainment of dry environmental air into the ascending cloud is assumed to take place in a succession of blobs. Time constants for different mixing processes are taken into account. They are compared with time constants for droplet evaporation or condensation and the impacts on droplet spectra are computed. If the time constant for droplet evaporation is small compared to that of the mixing process, the droplet spectra will adjust to the inhomogeneous humidity structures within the cloud.

The findings of Baker et al. (1984) together with the analysis of Paluch (1979) which suggests that in some cumuli the cloud air is a mixture from two sources—cloud base and cloud top—only, have been used to discuss observational results in a warm cumulus cloud (Jensen et al., 1985). They have tried to explain the observed different droplet concentrations at different heights with the fraction of cloud base air at these levels. All these hypotheses are very difficult to verify by measurements because it is almost impossible to sample the relevant parameters throughout the cloud with a resolution in time and space sufficient for fully revealing the mechanism of entrainment and mixing. It is the hope of the authors that the material presented in this article will contribute to the understanding of these mechanisms. Detailed observational data for a small warm growing cumulus cloud will be presented and discussed. They have been taken near cloud top during growth where an important part of the mixing process should be observable.

2. Measurements and strategy

The field observation programme KOOP (Konvection Oberpfaffenhofen) was set up to study the microphysics and dynamics of convective clouds in the lower Alpine Region near Oberpfaffenhofen. Cloud penetrations with the German Meteorological Research Aircraft FALCON-E (Meischner, 1985) enabled the simultaneous measurement of thermodynamical, dynamical and microphysical properties.

The case presented here is from 15 July 1982, where under generally anticyclonic conditions with light south-easterly winds, shallow cumulus clouds developed at noon over the northern foothills of the Alps. The base level was around 2675 m above mean sea level (MSL) and isolated tops up to 4100 m above MSL were observed during the period of observation. The altitude of the terrain is about 800 m above MSL with mountain peaks up to 1200 m above MSL.

The meteorological sounding taken at Munich, 100 km north-east from the observation site, shows only little instability near the ground and a small inversion at 650 hPa which corresponds to 3800 m above MSL. Above the inversion there is only a very slight decrease of humidity.

At 11:50:54 GMT we started ascending level scans about 175 m above cloud base when the depth of the selected cloud was $\sim$500 m, and increased flight altitude by steps of about 350 m up to about 1235 m above base. This uppermost level was near cloud top at a time of 32 min after the first penetration. Thus, we progressively observed the upper part of the growing cloud at four different levels. Efforts were continually made to fly through the central core of the cloud. Despite the south-easterly winds of 5–8 $\mathrm{m\,s^{-1}}$ blowing from the nearby Alps this cloud remained relatively stationary in location. Fig. 1 shows a plan view of the cloud traverses. Fig. 2 illustrates the lengths of the in-cloud flight tracks, the successive flight levels, as well as the time and direction of the penetrations. However, we would like to stress that this figure does not represent a snapshot of the cloud but rather it shows the development during a time interval of more than half an hour. This figure further illustrates the pronounced horizontal extent of the cloud. At the end of the observation time the cloud diameter was about twice the cloud depth. Fig. 3 visualizes the cloud dimensions and its upward growth during the observation time.

3. Instrumentation and data evaluation

The data recording equipment had a sampling rate of 10 Hz. The computer program used for calculating wind, temperature and humidity delivers one second averages of these quantities. Wind velocity is calculated from aircraft measurements using the equation

$$\boldsymbol{V}_{\mathrm{w}} = \boldsymbol{V}_{\mathrm{k}} - \boldsymbol{V},$$

where $\boldsymbol{V}_{\mathrm{w}}$ is the vector of wind velocity, $\boldsymbol{V}_{\mathrm{k}}$ the

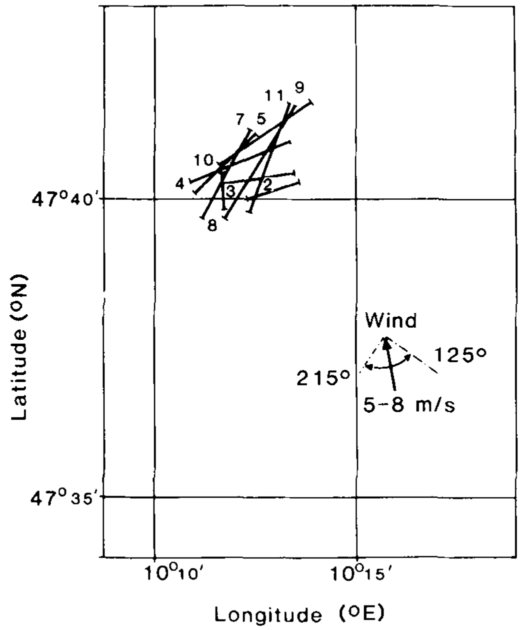

Fig. 1. Plan view of cloud traverses. The position of the respective traverse number indicates cloud entry.

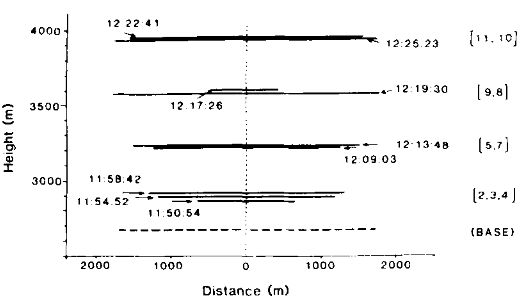

Fig. 2. Lengths and levels of successive flight paths within the cloud. Directions of penetration are indicated by an arrow, times are given in GMT. Note different scales for horizontal and vertical axes. Height is measured from mean sea-level.

velocity relative to the earth of a reference point on the aircraft, and V is the velocity of the same reference point relative to the undisturbed air. The two horizontal components of V_k are provided by the Litton LTN-72 inertial navigation system. The vertical component of V_k is calculated by differentiating the static pressure taking into account temperature, humidity and local acceleration of gravity. Values of the vertical component of V_k have to be filtered subsequently by a digital filter algorithm.

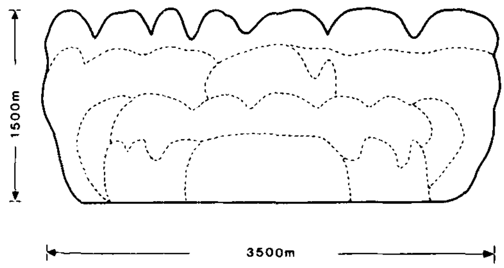

Fig. 3. Schematic view of the cloud observed showing its proportions with growth during the time of observation.

The equipment used for measuring the velocity V includes a Rosemount flow angle sensor forming the tip of the noseboom and the appropriate pressure transducers yielding static pressure, impact pressure and two differential pressures corresponding to the angle of attack and the angle of sideslip.

The temperature was measured by two Rosemount total temperature probes. Within cloud the temperature of such probes is reduced by the evaporation of water droplets, see Heymsfield et al. (1978). In this case the liquid water content was rather low, hence the temperature reduction is not expected to exceed 0.5 °C.

The humidity was measured with an ERC Lyman-α humidiometer mounted in a "humidity channel" within the aircraft nose. In general, the temperature in the humidity channel is higher than the free air static temperature, and often slightly exceeds the total temperature which in part is due to the fact that the inlet of the channel is formed by a total temperature probe housing. Therefore, within cloud the water droplets may evaporate inside the channel, which may cause the relative humidity to exceed 100% when it is reduced to free air conditions.

The droplet spectra were measured by a PMS droplet spectrometer FSSP-100. The size range covered for this flight was 5 μm to 33 μm in diameter and the resolution was 2 μm (Meischner, 1985).

4. Results

The calculated temperature, humidity and wind quantities will be plotted against time as one second means and the microphysical data as means over 0.1 s.

(1) *Potential temperature* (*TPOT*)
The relative accuracies are about ± 0.1 K in cloud-free air. The in-cloud accuracy is unknown but an error of not more than about -0.5 K seems possible due to the evaporation of droplets in the total temperature probe housing, see above.

(2) *Potential virtual temperature* (*TPV*)
Errors are somewhat higher than for TPOT.

(3) *Relative humidity* computed from Ly-α (*UWLY*)
The accuracy is $\sim 10\%$.

(4) *Water vapour mixing ratio* (*RLY*) computed from Ly-α values
The accuracy is $\sim 10\%$.

(5) *Horizontal wind speed* (*WIS*)
The relative accuracy is ± 0.5 m s^{-1}.

(6) *Wind angle* (*of horizontal wind*) (*WIA*)
The accuracy is $\sim \pm 10$ deg, depending on accuracy and amount of WIS. Owing to the averaging over one second the steps between 0° and 360° are slant which should not be misinterpreted as wind fluctuations.

(7) *Vertical wind speed* (*WWG*)
The absolute accuracy is ± 0.5 m s^{-1}, and the relative accuracy ± 0.2 m s^{-1}.

(8) *Cloud droplet concentration* (*CONC*)
The accuracy is $\pm 17\%$.

(9) *Mean droplet diameter* (*MDIAM*)
The accuracy is ± 1 μm.

(10) *Liquid water content* (*LWCKN*) computed from droplet spectra
The accuracy is $\pm 35\%$.

(11) *Dispersion of droplet spectra* (*DIS*)
The error is $\sim 10\%$. Note that the lower cut-off of the distribution is at 5 μm.

The time-dependent plots of microphysical data do not depict the actual shapes of individual spectra such as spectral width or multiple-peaked structures.

We therefore use an additional much more suggestive presentation. A series of droplet distribution functions at successive times t_1, t_2, t_3 ... are converted into contour plots as illustrated in Fig. 4. The number concentrations of the spectra in this figure are marked by four equal steps and the intersection points are projected on the diameter axis. These projections are then transferred to a diameter-versus-time presentation and points of equal number concentration levels are connected. These diameter-versus-time contour plots clearly illustrate spectral properties such as spectral width, maximal diameter, peak of spectra, skewness and multiple-peaked spectra. These plots are very helpful in surveying variations in the microphysical behaviour against the thermo-dynamical or dynamical properties.

Some typical cloud cross sections—one for each flight level—are selected for presentation and discussions. These are [2], [7], [9], [11], see Figs. 1, 2.

4.1. *Penetration at 2850 m above MSL from west to east*

Figs. 5a, b, penetration [2], represent a very homogeneous part of the cloud. The updraft acquired a peak value of 6 m s^{-1} and a downward motion of 1 m s^{-1} was observed at the western edge outside the cloud. Droplet populations were encountered for updraft velocities exceeding 1.5 m s^{-1} at the western edge and 2.5 m s^{-1} at the eastern edge. The relative humidity displays rather constant values in excess of 100% for the whole cloud extent. The area of positive buoyancy, indicated by an increase of TPV of 1 K extends beyond the western edge of the cloud to the downdraft region.

The environmental wind speed was around 6 m s^{-1}, it decreased within the cloud to values around 3 m s^{-1} and the wind direction changed from south-east to fluctuating easterly directions. The droplet spectra were very homogeneous, the LWC of 0.35 g/m^3 decreased only slightly from west to east corresponding mainly to a decrease in mean diameter. The droplet spectra contour plot illustrates prominently the homogeneity, which corresponds to a constant dispersion of about 0.3.

4.2. *Penetration at 3240 m above MSL from north-east to south-west*

As seen in Figs. 6a, b, representing penetration [7], the overall structure is rather inhomogeneous. There are two updraft peaks, one reaching nearly 8 m s^{-1} in the eastern part and the other 4 m s^{-1} in the western part. At both sides outside the cloud, downward motion of 1 m s^{-1} for regions each about 400 m wide was observed. Droplets were found for updraft velocities of more than 1 m s^{-1}. The in-cloud humidity field fluctuates

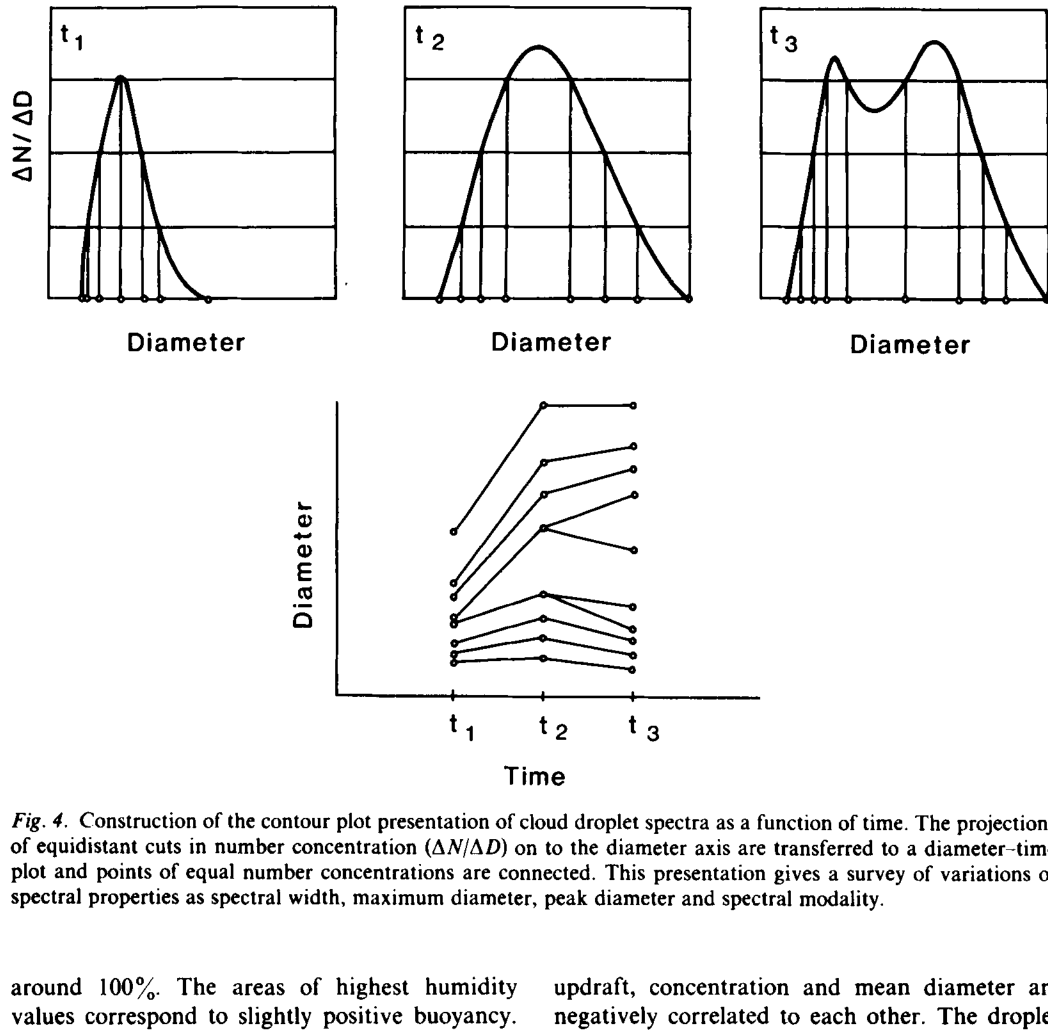

Fig. 4. Construction of the contour plot presentation of cloud droplet spectra as a function of time. The projections of equidistant cuts in number concentration ($\Delta N/\Delta D$) on to the diameter axis are transferred to a diameter–time plot and points of equal number concentrations are connected. This presentation gives a survey of variations of spectral properties as spectral width, maximum diameter, peak diameter and spectral modality.

around 100%. The areas of highest humidity values correspond to slightly positive buoyancy. In this case they are not all strongly related to the updraft peaks except for the main peak. The horizontal wind speed almost completely breaks down near the main updraft peak. The wind direction changes from south via west to nearly north (opposite direction) inside the cloud, which is significantly different from the other traverse at this level, where it veers from south to easterly directions within the cloud. The microphysical properties were rather inhomogeneous. The droplet number concentration decreases significantly for areas of low humidity. The LWC follows the variations in mean droplet diameter which is positively correlated with updraft velocity, humidity and buoyancy as observed for most penetrations. In the areas of the strongest updraft, concentration and mean diameter are negatively correlated to each other. The droplet spectra dispersion fluctuates between 0.3 and 0.4.

The inhomogeneous microphysical structure is again illustrated by the corresponding droplet spectra contour plot. This additionally shows bimodality of spectra around 12:13:53–54 and 12:13:61 GMT which is on both flanks of the strong updraft core.

4.3. Penetration at 3570 m above MSL from north-east to south-west

On this flight path, penetration [9], we observed 3 updraft maxima of 4.5 and 6 $m s^{-1}$ respectively as can be seen in Figs. 7a, b. North-east of the cloud a 2000 m wide region of downward motion can be recognized. The southerly wind direction of the environment was

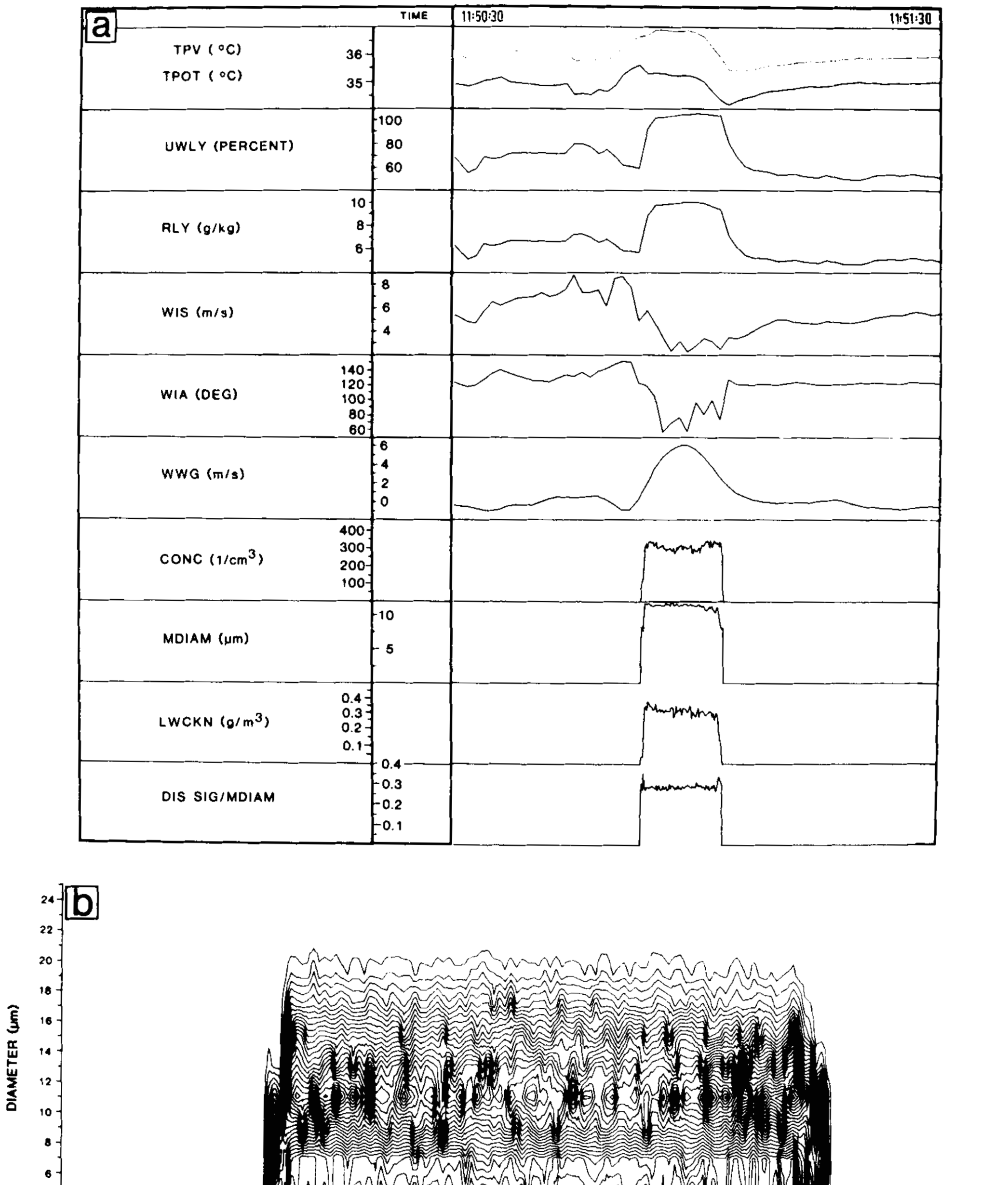

Fig. 5. (a) Penetration [2] from west to east at 2850 m above MSL at 11:50:54 GMT. Dynamical, thermodynamical and cloud droplet spectral properties near cloud base, as explained in 4. (b) Corresponding contour plot of cloud droplet distributions.

maintained within one half of the cloud. In the region of the peak upward velocities, however, strong fluctuations in wind direction and speed, which almost fully broke down near the peaks, were observed. The cloudy air in the north-east extended about 200 m into the region of down-

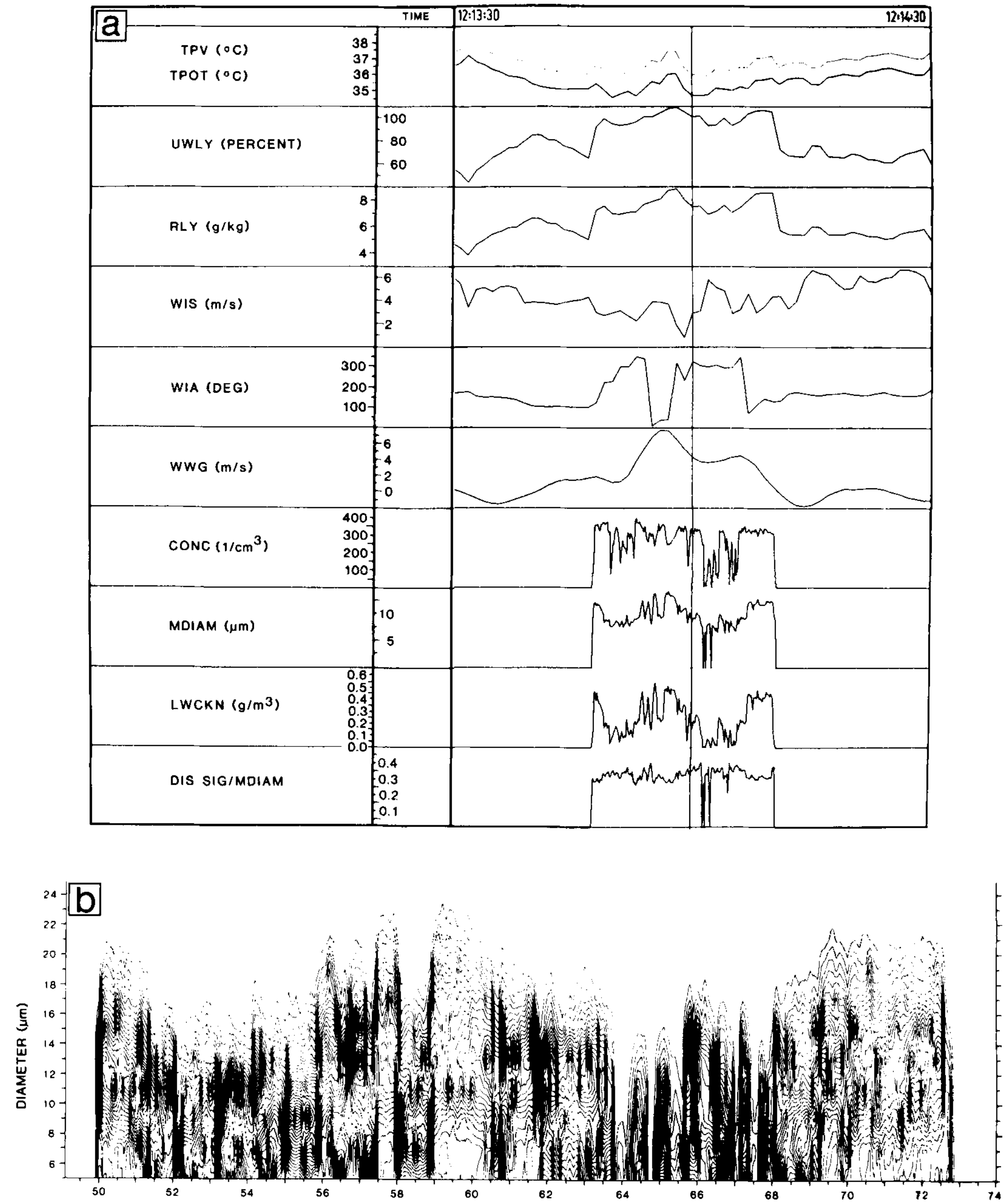

Fig. 6. (a) As in Fig. 5a but for penetration [7] at 3240 m above MSL at 12:13:48 from north-east to south-west. (b) As in Fig. 5b but for penetration [7].

ward motion. Within this small distance the mean droplet diameter and the LWC decrease, whereas the concentration and dispersion remain essentially constant and buoyancy increases. This suggests that a parcel out of the rather homogeneous cloud air was descending adia-

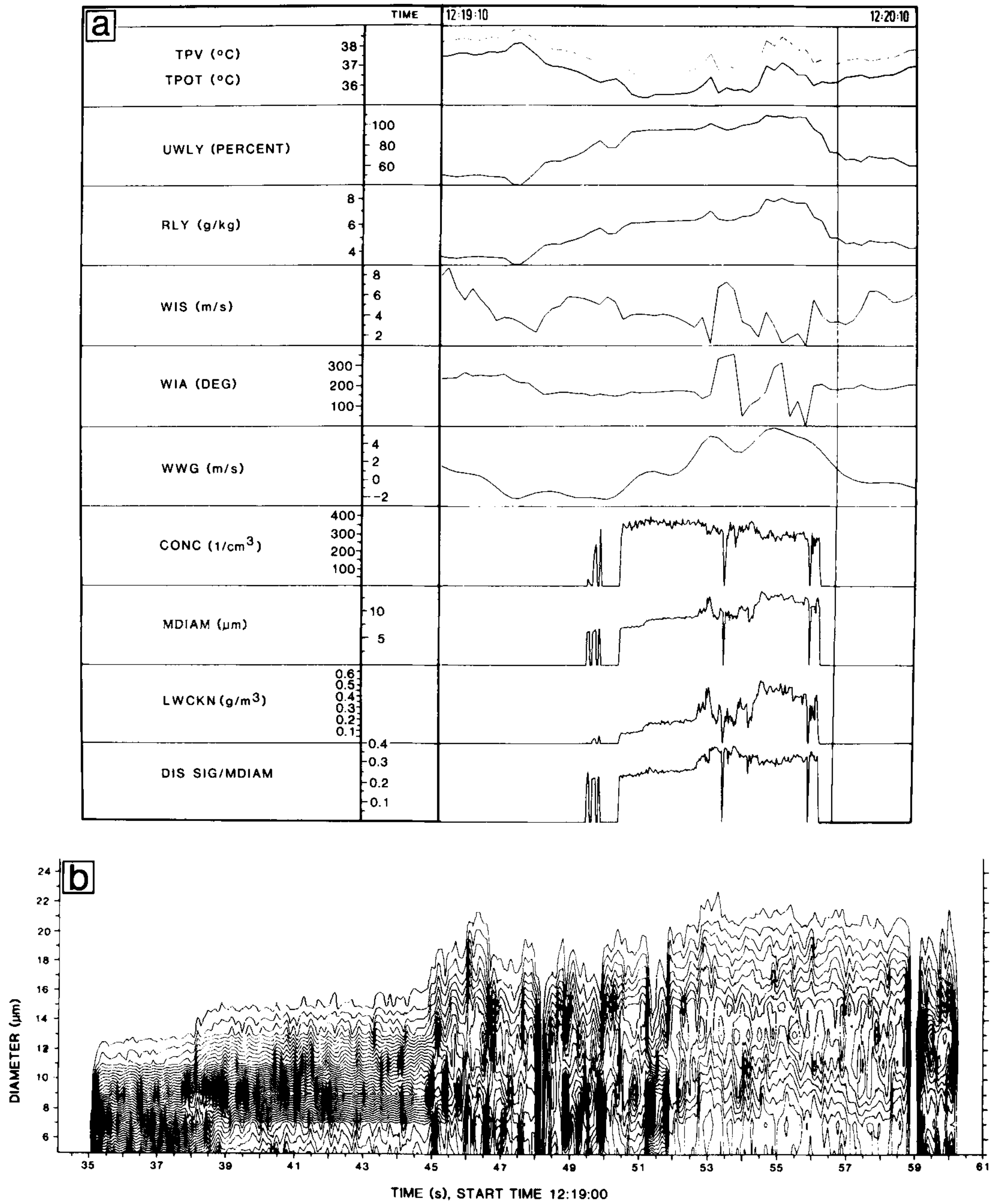

Fig. 7. (a) As in Fig. 5a but for penetration [9] at 3570 m above MSL at 12:19:30 GMT from north-east to south-west. (b) As in Fig. 5b but for penetration [9].

batically with all droplets evaporating in a manner so that they all lost the same fraction of their diameter (cf. Jensen et al., 1985). The humidity increased from north-east to south-west in a rather smooth curve. The mean droplet diameter follows the updraft velocity, humidity and buoyancy. The mean diameter and the concentration were negatively correlated to each

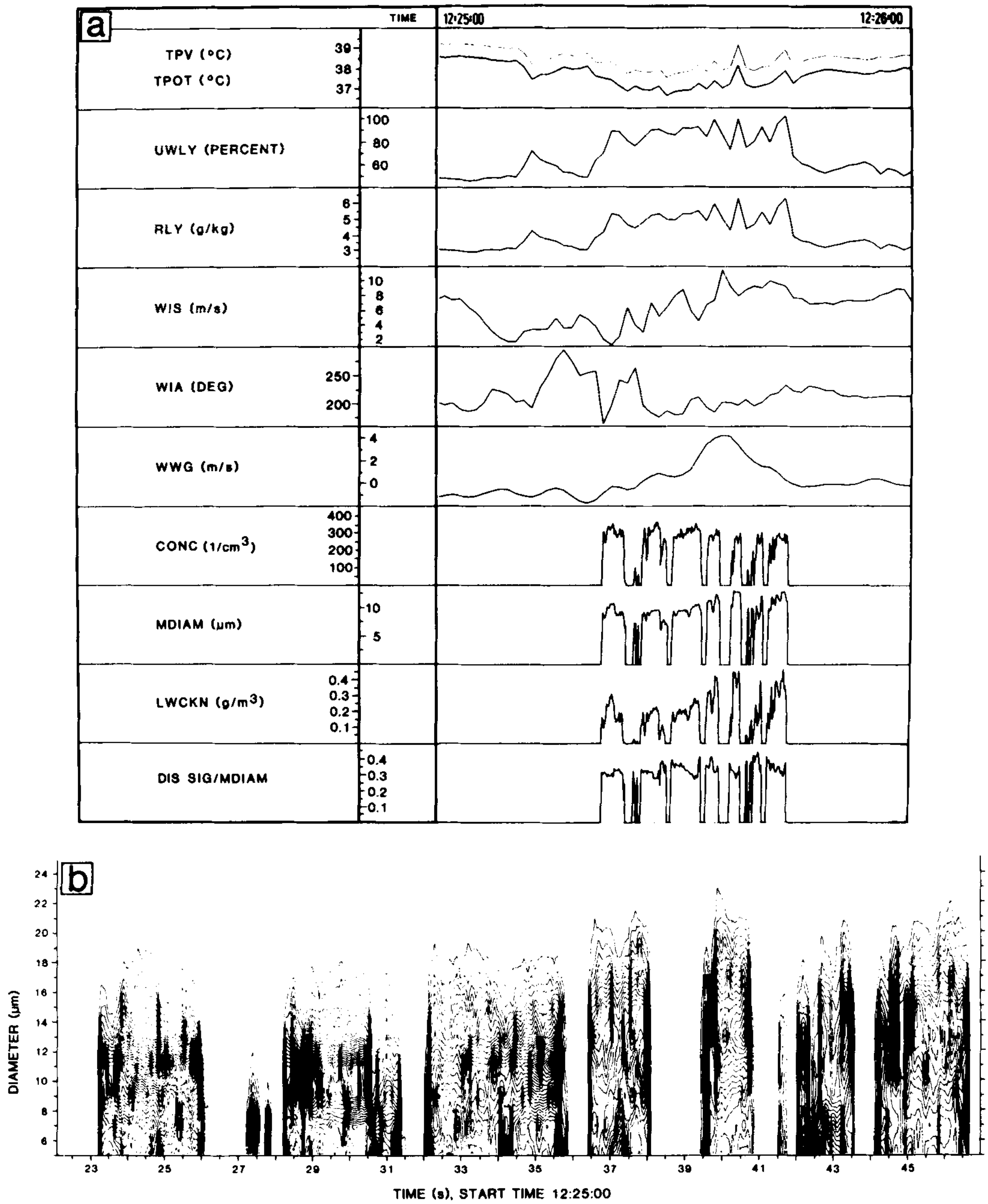

Fig. 8. (a) As in Fig. 5a but for penetration [11] at 3910 m above MSL at 12:25:23 GMT from north-east to south-west. (b) As in Fig. 5b but for penetration [11].

other within the strong updrafts. The dispersion ranges between 0.25 and 0.35. The dispersion is negatively correlated to the mean diameter in the strong updraft regions. Near the cloud center strong fluctuations in mean diameter and dispersion were observed. The contour presentation of droplet spectra gives more insight into the homogeneity of the droplet spectra. Some locations of bimodality are discernible near 12:19:46.5; 12:19:48.5 and 12:19:57 GMT.

4.4. Penetration at 3910 m above MSL from north-east to south-west

For this flight section [11] (see Figs. 8a, b) the cloud was heavily structured presenting the "cauliflower" structure at the top of a growing cumulus cloud with individual small towers of about 200 to 600 m in diameter each. The maximum updraft speed was 4 ms^{-1}. The wind speed within the cloud exceeded the environmental wind speed on the upshear side and decreased with strong fluctuations to almost zero downwind. The environmental wind blew from southerly directions at 6 to 8 ms^{-1}. Only small areas of cloudy air near the updraft peak were positively buoyant. These local peaks in buoyancy correspond to maxima of humidity which only at these points reached 100%. The humidity fluctuated prominently between 100% and less than 80%. These variations were accompanied by corresponding changes in the droplet concentration and the mean diameter. For the cloud on the whole, an increase of the mean diameter was coupled with a reduction in concentration; this trend, however, contrasts with the behaviour within the individual small "parcels" where these two quantities change in the same sense. The dispersion of droplet spectra fluctuated opposite to the mean diameter for the whole cloud as well as for the individual cloud parcels.

The droplet spectra contour plot shows the frequent occurrence of bimodal spectra preferentially at the centers of the individual parcels. An enlarged contour plot of the central individual small tower is given in Fig. 10 (see Section 5).

5. Discussion

The non-precipitating cumulus cloud investigated by aircraft probing was rather shallow. At the beginning of measurements it was approximately 2500 m in diameter and about 500 m in depth and during the observation period of 36 minutes it developed a depth of 1500 m and a diameter of 3500 m, measured at the top. Because of these dimensions, the surface of this cloud remained large in relation to its volume and this caused intense interaction with environmental air especially at the upward moving upper surface. The entrained air did not form penetrative downdrafts for, with the exception of traverse [10] which was nearest to the tops, there was no significant downdraft encountered within the cloud. Instead, the local environmental air was engulfed at the upper surface and carried aloft by the ascending cloud. The other source of entrained air was a considerable horizontal inflow, observable at traverses [8] to [11] (see Figs. 7, 8) which were oriented more or less up- or downwind (see Table 1).

The frequent occurrence of negative buoyancy in the ascending cloud air illustrates the intensity of the mixing process. Only the updraft peaks are linked with clearly positive buoyancies.

The wind field within the cloud was at first characterized by one broad updraft core with speed values up to 6 ms^{-1}. From the fourth penetration after 8 min of observation time, the updraft was observed to become more structured with up to three maxima along the flight track. While the environmental wind speed was at least 5 ms^{-1}, the cloud remained stationary during the whole measurement period. The horizontal wind speed broke down or was substantially lowered at, near or behind the updraft maxima. So we can state that the cloud acted as an obstacle for the environmental wind. One mechanism by which this could have been achieved is vertical rotation which can be inferred especially from the reversal of the horizontal wind at traverse [7] (Fig. 6).

Figs. 5–8 represent the 4 different levels in which all cloud penetrations were performed (see Table 1 for a survey). The data from these levels offer the possibility for some quantitative considerations. Among all the penetrations traverse [2] (Fig. 5) shows the most homogeneous conditions and the highest total water mixing ratio. So we assume that at traverse [2] we encountered undiluted cloud air and hence take it as a reference for calculations of adiabates. If we compute the reversible moist adiabat starting from traverse [2] we get values of temperature and LWC which are far above the measured maxima of traverses [7], [9] and [11] (see Table 2). The cloud base is found to be 175 m below traverse [2].

Thus, we must state that we did not encounter an undiluted moist adiabatic core above traverse [2]. We now compute the mass fraction f of the

Table 1. *Altitude, length, direction and time difference of aircraft traverses through cloud, in-cloud and environmental wind*

Traverse No.	Altitude (m)	Length of traverse (km)	Mean vertical wind speed ($m s^{-1}$)	Maximum vertical wind speed ($m s^{-1}$)	Mean wind angle (deg.)	Mean horizontal wind speed ($m s^{-1}$)	Aircraft heading (deg.)	Environ-mental wind angle (deg.)	Environ-mental wind speed ($m s^{-1}$)	Time difference (min)
2	2850	1.3	+4.51	6.13	87.8	3.12	73	125	5–7	0
3	2860	2.36	+2.39	4.67	109.6	2.59	80	125	5–7	4.0
4	2890	2.62	+2.40	4.14	83.8	3.17	68	125	5–7	7.9
5	3220	2.48	+3.56	6.71	72.1	1.57	224	165	6	18.1
7	3240	3.04	+3.90	7.64	334.3	1.24	210	160	5–7	23.0
8	3590	0.87	+4.05	6.04	183.0	3.04	355	200	5–7	26.5
9	3570	3.55	+3.13	5.77	166.1	1.12	211	200	5–8	28.9
10	3920	3.15	−0.11	1.80	219.9	7.01	54	210	6–8	31.7
11	3910	3.50	+1.45	4.23	203.0	6.68	200	215	6–8	34.7

The traverses 2, 7, 9 and 11 are presented in detail in Subsections 4.1 to 4.4 and Figs. 5–8.

Table 2. *Thermodynamic and microphysical quantities*

Traverse No.	Altitude (m)	Pressure (hPa)	Measured tempera-ture (°C)	Moist adiabatic tempera-ture (°C)	Dry adiabatic tempera-ture (°C)	Adiabatic LWC (g/m^3)	Maxi-mum measured LWC (g/m^3)	Maxi-mum measured LWC-mixing ratio (g/kg)	Satu-ration mixing ratio (g/kg)	Droplet concen-tration ($1/cm^3$)	Droplet concen-tration (1/mg)
base	2675	742.0	—	9.07	9.98	0	—	—	9.85	—	—
2	2850	725.8	8.20	8.20	8.20	0.327	0.35	0.39	9.49	323	362
7	3240	692.7	5.25	6.31	4.48	0.961	0.50	0.58	8.10	354	411
9	3570	666.6	3.06	4.74	+1.46	1.429	0.50	0.60	7.20	370	442
11	3910	637.3	+0.30	2.87	−2.04	1.919	0.43	0.54	6.17	323	400

The values of traverse [2] are taken as a reference for dry and moist adiabatic calculations. The values of the cloud base are calculated assuming moist adiabatic ascent of the cloud air from the base to the level of traverse [2].

original cloud air (from traverse [2]) in the updraft core of the more elevated traverses, where the local maximum of total water mixing ratio occurs. For traverse [7] we use the formula

$$f_{2,7} = \frac{r_{c7} - r_{e2,7}}{r_{c2} - r_{e2,7}},$$

where $f_{2,7}$ is the mass fraction of the air from traverse [2] in the parcel with the highest total water mixing ratio of traverse [7], r_{c2} and r_{c7} are the total water mixing ratios at traverse [2] and in the updraft core of traverse [7] respectively, and $r_{e2,7}$ is the mean mixing ratio in the environmental layer between traverses [2] and [7]. This layer is the only possible source of entrained air in this case. Extracting the appropriate values from Table 2 and from Figs. 5a and 6a (for $r_{e2,7}$) we get

$$f_{2,7} = \frac{8.7 - 5.5}{9.9 - 5.5} = 0.73;$$

similarly for traverse [9]:

$$f_{7,9} = \frac{7.8 - 4.3}{8.7 - 4.3} = 0.80,$$

$$f_{2,9} = f_{2,7} * f_{7,9} = 0.58,$$

and for traverse [11]

$$f_{9,11} = \frac{6.7 - 4.0}{7.8 - 4.0} = 0.71,$$

$$f_{2,11} = f_{2,7} * f_{7,9} * f_{9,11} = 0.41.$$

Thus, at traverse [11], only 41% of the air in the parcel with the highest total water mixing ratio originate from the undiluted cloud air of traverse [2]. Using the droplet concentrations per mass unit (1 mg) in Table 2 we can easily compute the fraction $f_{d2,11}$ of the original droplets from traverse [2] in the above-mentioned parcel of traverse [11]:

$$f_{d2,11} = \frac{235 \text{ mg}^{-1} \bullet 0.41}{260 \text{ mg}^{-1}} = 0.37.$$

The result is that at most 37% of these droplets could have originated from traverse [2] (if all droplets had been conserved). By the formation of so many new droplets bimodal spectra can easily arise.

If we compute, in the same manner as above, the average mass fractions $\bar{f}$ of original cloud air over the whole traverses, we get

$$\bar{f}_{2,7} = 0.57,$$

$$\bar{f}_{2,9} = 0.31,$$

$$\bar{f}_{2,11} = 0.15,$$

which means that, e.g., along traverse [11] 85% of the cloud air had been mixed in from the environment.

Assuming that traverses [3] and [9] were at the same distance (about 300 m) from the actual tops, then the cloud had grown by 710 m within 1490 s (see Table 1). This results in an average vertical growth speed of 0.48 m s^{-1}. On the other hand, the vertical speed of the cloud air, averaged over traverses [3], [7] and [9] (Table 1) is about 3.14 m s^{-1}. Thus, we have an average upward speed of 2.66 m s^{-1} relative to the upper boundary of the cloud. Taking a mean cloud diameter of 3 km, this corresponds to an ascending volume of $18.8 * 10^6 \text{ m}^3 \text{s}^{-1}$. This volume in part serves for broadening the cloud. The rest must have been leaving the cloud through the boundaries above the traverse. Assuming that the cloud diameter had grown by 1 km within 1400 s (cf. Table 1), we get a mean radial growth speed of 0.36 m s^{-1}. On the other hand, if the whole ascending volume would leave the cloud sidewards (through a cylinder 300 m high and 3 km in diameter) we would have a mean relative radial wind speed of

$$\frac{18.8 \times 10^6 \text{ m}^3 \text{s}^{-1}}{\pi \times 3000 \text{ m} \times 300 \text{ m}} - 0.36 \text{ m s}^{-1}$$

$$= 6.65 \text{ m s}^{-1} - 0.36 \text{ m s}^{-1} = 6.3 \text{ m s}^{-1}.$$

No such speed was observed. So we must conclude that the ascending surplus air was leaving the cloud in a layer about the tops. From the above values we estimate that between traverses [3] and [9] 15% of the ascending cloud air was used for the vertical and about 5% for the lateral growth of the cloud, whereas 80% was detrained from the cloud.

The microphysical properties were mainly determined by the degree of mixing of the cloudy air with environmental air. Two distinctly different structures were observed for each traverse characterizing the whole upper observed part of the cloud as it developed. These structures may be called "homogeneous" and "inhomogeneous" with respect to microphysics. The homogeneous regions correspond to what is called a "smooth" region by Austin et al. (1985) and Blyth and Latham (1985).

The *homogeneous parts* are characterized by maximal relative humidities near 100%, positive buoyancies and significant upward motion of 4 m s^{-1} and more. They are relatively uniform in droplet spectral characteristics. Corrected droplet concentrations were found to be around 320 cm^{-3} and no significant change with cloud depth was observed. Local variations in LWC were mainly due to variations in mean droplet diameter. The maximum LWC calculated from droplet spectra is found to be 0.5 g m^{-3} at the upper levels and about 0.35 g m^{-3} at lower levels at the earlier times of observation.

Within the homogeneous parts the mean droplet diameter and the number concentration are correlated negatively which is most clearly seen with traverses [3], [4], [5] and [9], see Fig. 7. This suggests that condensational as well as coalescence processes were involved. The fact that the dispersion of the droplet spectra decreases with increasing mean droplet diameter argues for condensational growth whereas the decrease of number concentration with increasing diameter argues for growth by coalescence.

Beside these more or less homogeneous parts, certain areas of the cloud were found to be very *inhomogeneous* with respect to microphysics. They were heavily influenced by mixing with dry environmental air causing significant water vapour undersaturation. As oberved, this results in evaporation with the consequence that both droplet number concentration *and* mean droplet diameter are reduced. The change in the slopes of the droplet size distribution functions are emphasized by the mean diameter, the dispersion, and most impressively of all, in the corresponding contour representations.

Evaporation causes cooling and a decrease in buoyancy. The measurements show that the positive momentum of the upwards developing cloud is always too great to allow the negatively buoyant cloudy air to form penetrative downdrafts. These negatively buoyant parcels were pushed upwards together with the whole cloud volume.

An overview of the values for humidity, UW, buoyancy, Buoy, and vertical velocity, w, separated for the homogeneous and inhomogeneous cloud parts for all traverses are given in Tables 3, 4, respectively. The values are roughly classified as explained in the caption. They show that the inhomogeneous parts are characterized by significant water vapour undersaturation and negative buoyancy but with nearly always upward motion. Some inhomogeneous parts were found to move downwards only at cloud top near the end of the observation time for traverse [10]. The homogeneous parts near the maxima of upward motion typically show water vapour saturation and mainly positive or neutral buoyancy. At the last penetrations, [10] and [11], near the top, undersaturation and negative buoyancies were observed for homogeneous cloud parts indicating the end of cloud growth at cloud top. The ratio of homogeneous to inhomogeneous cloud sections was found to be roughly one to one.

The dispersion of droplet spectra as a measure of its width should increase with progression of droplet growth and hence the dispersion should increase with cloud depth. The observed disper-

Table 3. *Classification of humidity UW, buoyancy Buoy and vertical velocity W for the microphysically homogeneous cloud parts of each traverse*

Traverse	UW	Buoy	W
[2] 1	↑	↑	↑↑
[3] 1	↑	↑	↑↑
2	↑	–	↑↑
[4] 1	↓	–	↑
2	↑	↑,↓	↑↑
3	↑	↑	↑↑,↑
[5] 1	↑,↓	↑,↓	↑↑
2	↑	↓,–	↑↑
[7] 1	↑	↑	↑↑
2	↑	↑,–	↑↑,↑
[8] 1	↑	↑	↑↑
[9] 1	↓	↓	↑↑,↑
2	↑	↑	↑↑
[10] 1	↑,↓	↑,↓	↑
2	↑	–	↑
[11] 1	↓	↓	↑,↓
2	↓	↓	↑
3	↓	↓	↑,↑↑
4	↑	–	↑↑
5	↑	↑	↑↑
6	↑	↑	↑

For UW ↑ means near saturation, ↓ some % less than maximum, and ↓↓ more than about 5% undersaturated.

For Buoy ↑ means positive, – neutral, and ↓ negative.

For W ↑↑ means more than 2 $m s^{-1}$ upwards, ↑ 0–2 $m s^{-1}$ upwards, and ↓ 0–2 $m s^{-1}$ downwards.

Table 4. *As in Table 3 but for the microphysically inhomogeneous cloud parts of each traverse*

Traverse	UW	Buoy	W
[2] 1	homogeneous		
[3] 1	↓↓	↓	↑↑
2	↓↓	–	↑
[4] 1	↓↓	↓	↑↑
2	↓↓	–	↑
[5] 1	↓↓	↓	↑↑
[7] 1	↓↓,↓	↓,↑	↑,↑↑
2	↓↓,↓	↓	↑↑
[8] 1	↓↓	↓	↑↑
[9] 1	↓↓	–	↓
2	↓↓	–	↑↑
[10] 1	↓↓	–	↓
2	↓↓	↓	↑,↓
[11] 1	↓↓	↓	↑
2	↓↓	↓	↑

sion for the increasing flight levels are shown and compared with findings of Warner (1969) in Fig. 9. The trends correspond with each other.

Bimodal spectra have been observed for the traverses [5], [7], Fig. 6, [9], [10] and most frequently for [11], Fig. 8. For the traverses [5], [7] and [9], isolated small areas of bimodality were found within the microphysically more homogeneous parts. The measurements show that caution is necessary in discussing the modality of cloud droplet spectra in a cumulus cloud. A very frequent spatial alteration of areas with monomodal spectra having quite different peak diameters may occur. This may be misinterpreted as bimodal spectra if too long a distance is averaged. Fig. 10 gives an example of a central cloudy volume of traverse [11]. For the time interval between 12:25:33 and 12:25:34.5, frequent fluctuations in peak diameter were observed to be changing within a distance of 20 m, whereas between 12:25:34.5 and 12:25:35.5 a real bimodal structure is evident.

Nowhere within the cloud was a liquid water content of 0.52 gm^{-3} surpassed. On the other hand, the calculation of the moist adiabatic process (starting from traverse [2], see Table 2) gives an LWC of 1.92 gm^{-3} for traverse [11]. From Table 2 one realizes that the moist adiabatic LWC difference is about 0.50 for an altitude difference of 350 m (one-third of the difference between traverses [2] and [11]). Therefore, an originally saturated air parcel can ascend by 350 m at most, before its LWC no longer rises, i.e., before it is fully mixed up with drier air. The mean vertical speed in the updraft core was about 5 ms^{-1}. So we can estimate a characteristic time τ_T for turbulent mixing:

$$\tau_T \approx 350 \text{ m}/(5 \text{ ms}^{-1}) = 70 \text{ s}.$$

According to Jensen et al. (1985), the following relation holds for normal continental cumuli:

$$\tau_k \ll \tau_r \ll \tau_T,$$

where τ_k and τ_r are the characteristic times for homogenization by molecular diffusion (of an eddy of the Kolmogorov scale) and for droplet evaporation, respectively. This relation is confirmed by the observed adjustment of the droplet spectra to the inhomogeneous humidity distribution.

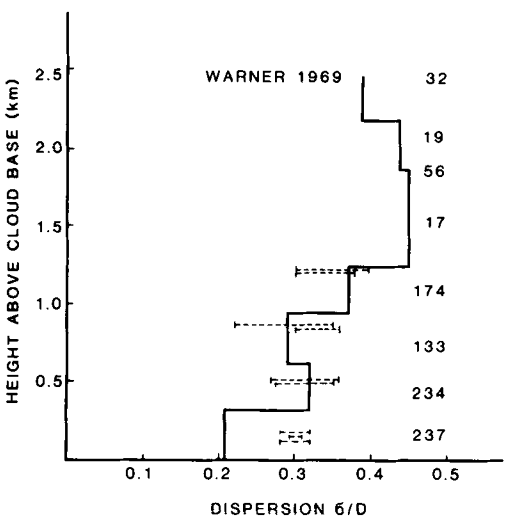

Fig. 9. Dispersions of observed cloud droplet spectra—defined as standard deviation over mean diameter—with height above cloud base shown as dotted lines. They visualize the variance of the dispersions for the whole traverse. The solid line represents measurements of Warner (1969) giving means of a number of impact samples as indicated on the right.

6. Summary and conclusions

The growing cloud, sampled at four different levels remained stationary during the sampling period in an environmental wind field of 5 to 8 ms^{-1}. The liquid water content was substantially below the adiabatic values everywhere above the lowest penetration level. The entrained air was found to originate from the upwind side and from local air engulfed by the ascending cloud at its upper boundary. At the highest penetration level only 15% of the cloud air (averaged over the whole traverse) consisted of cloud air from the base. On the other hand, there was a substantial detrainment. 80% of the ascending cloud air must have been leaving the cloud mainly from the layer about the tops. On the average the cloud was undersaturated along all traverses except [2]. Therefore, the cloud should have decayed very quickly as soon as the upward movement ceased.

A characteristic time of turbulent mixing was derived from a comparison of calculated adiabatic and measured liquid water content.

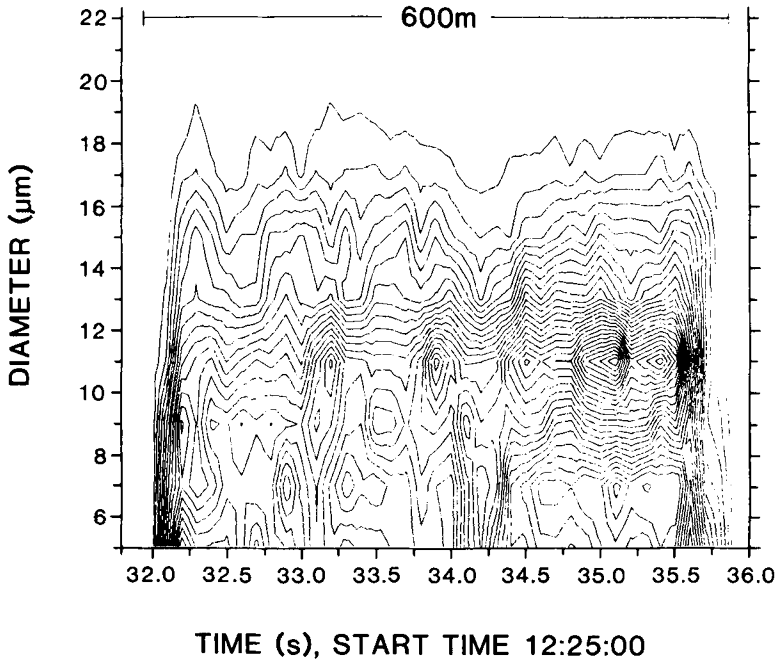

Fig. 10. Enlarged cloud droplet spectra contour plot for a central cloud parcel of traverse [11]. It shows the high spatial variability of spectral characteristics including bimodality in the intervals between 12:25:34.5 and 12:25:35.5. Maximum $N = 59$ for the 2 μm diameter interval, 30 cuts.

No evidence for mixing by "penetrative downdrafts" was found since w was mostly positive. The continuous mixing during growth caused widespread regions of undersaturation linked to negative buoyancies.

The response of the cloud microphysics resulted in a distinctly inhomogeneous structure. Only parts with high humidities, linked with positive buoyancies and the strongest upward motions observed, can be described as being of a microphysically rather homogeneous structure, even though very small scale variations of droplet spectral shape were observed in these parts too. The LWC is mainly determined by the mean droplet diameter. A presentation of cloud droplet spectra against time as contour plots shows the small-scale variability. These small-scale mixing processes that were observed from a very early state of convective cloud development seem to be of fundamental importance for the further growth (Klaassen and Clark, 1985).

Future aircraft observations should provide more detailed information on the wind velocity field including rotation, the mass exchange and mass budget, the origin of entrained air, the outflow of detrained air, and the mixing process. Such data are necessary not only for a better understanding of the formation of clouds and precipitation (Reuter, 1986), but also for the prediction of the scavenging or transformation of atmospheric pollution by clouds and precipitation.

7. Acknowledgements

We would like to thank our flight facility, especially, H. G. Christner and R. Rahn for their efficient navigation through all the nebulous elements as clouds, limitations by air traffic control and aircraft flight restrictions. We also greatly appreciate the contributions of H. Fimpel, H. Horst, K. Kugler, R. Roth, C. Rox and G. Wilke to the Falcon measuring system. Further thanks are due to Th. Jank and H. Löffler for their support in data evaluation and software programming. Stimulating discussions with T. Clark, Th. Hauf and P. Wendling and their reading of the manuscript is greatly appreciated. Thanks are also due to Gisela Gersing and Evi Schmidt for carefully typing the manuscript and G. Jacob for preparing the drawings.

REFERENCES

Austin, P. H., Baker, M. B., Blyth, A. M. and Jensen, J. B. 1985. Small-scale variability in warm continental cumulus clouds. *J. Atmos. Sci. 42*, 1123–1138.

Baker, M. B. and Latham, J. 1979. The evolution of droplet spectra and the rate of production of embryonic raindrops in small cumulus clouds. *J. Atmos. Sci. 36*, 1612–1615.

Baker, M. B. and Latham, J. 1982. A diffusive model of the turbulent mixing of dry and cloudy air. *Q. J. R. Meteorol. Soc. 108*, 871–898.

Baker, M. B., Corbin, R. G. and Latham, J. 1980. The influence of entrainment on the evolution of cloud droplet spectra: I. A model of inhomogeneous mixing. *Q. J. R. Meteorol. Soc. 106*, 581–598.

Baker, M. B., Blyth, A. M., Carruthers, D. J., Caughey, S. J., Choularton, T. W., Conway, J., Fullarton, G., Gay, M. J., Latham, J., Mill, C. S., Smith, M. H. and Stromberg, I. M. 1982. Field studies of the effect of entrainment upon the structure of clouds at Great Dun Fell, *Q. J. R. Meteorol. Soc. 108*, 899–916.

Baker, M. B., Breidenthal, R. E., Choularton, T. W. and Latham, J. 1984. The effects of turbulent mixing in clouds. *J. Atmos. Sci. 41*, 299–304.

Blyth, A. M. and Latham, J. 1985. An airborne study of vertical structure and microphysical variability within a small cumulus. *Q. J. R. Meteorol. Soc. 111*, 773–792.

Blyth, A. M., Choularton, T. W., Fullarton, G., Latham, J., Mill, C. S., Smith, M. H. and Stromberg, I. M. 1980. The influence of entrainment on the evolution of cloud droplet spectra: II. Field experiments at Great Dun Fell. *Q. J. R. Meteorol. Soc. 106*, 821–840.

Heymsfield, A. J., Dye, J. E. and Biter, C. J. 1978. Overestimates of entrainment from wetting of aircraft temperature sensors in cloud. *J. Appl. Meteorol. 18*, 92–95.

Jensen, J. B., Austin, P. H., Baker, M. B. and Blyth, A. M. 1985. Turbulent mixing, spectral evolution and dynamics in a warm cumulus cloud. *J. Atmos. Sci. 42*, 173–192.

Jonas, P. R. and Mason, B. J. 1982. Entrainment and the droplet spectrum in cumulus clouds. *Q. J. R. Meteorol. Soc. 108*, 857–869.

Klaassen, G. P. and Clark, T. L. 1985. Dynamics of the cloud-environment interface and entrainment in small cumuli: Two-dimensional simulations in the absence of ambient shear. *J. Atmos. Sci. 42*, 2621–2642.

La Montagne, R. G. and Telford, J. W. 1983. Cloud top mixing in small cumuli. *J. Atmos. Sci. 40*, 2148–2156.

Meischner, P. (ed.) 1985. User's manual for the Falcon-system. *ESA-TT-936*.

Paluch, I. R. 1979. The entrainment mechanism in Colorado cumuli. *J. Atmos. Sci. 36*, 2467–2478.

Reuter, G. W. 1986. A historical review of cumulus entrainment studies. *Bull. Am. Meteorol. Soc. 67*, 151–154.

Telford, J. W. and Chai, S. K. 1980. A new aspect of condensation theory. *Pageoph 118*, 720–742.

Telford, J. W. and Wagner, P. B. 1980. The dynamical and liquid water structure of the small cumulus as determined from its environment. *Pageoph 118*, 935–952.

Telford, J. W. and Wagner, P. B. 1981. Observations of condensation growth determined by entity type mixing. *Pageoph 119*, 934–965.

Warner, J. 1969. The microstructure of cumulus cloud. Part I. General features of the droplet spectrum. *J. Atmos. Sci. 26*, 1049–1059.